RSC Advances

ROYAL SOCIETY OF CHEMISTRY

PAPER

View Article Online
View Journal | View Issue

Check for updates

Cite this: *RSC Adv.*, 2024, **14**, 13984

Non-thermal plasma modulated L-tyrosine self-assemblies: a potential avenue for fabrication of supramolecular self-assembled biomaterials†

Priya Bhatt,[ab] Prajakta Sharad Garad,[c] V. V. S. Prasanna Kumari Rayala,[d] P. Radhakrishnanand[d] and Kamatchi Sankaranarayanan *[a]

Received 12th March 2024
Accepted 22nd April 2024

DOI: 10.1039/d4ra01891e

rsc.li/rsc-advances

Aromatic amino acids (AAs) have garnered particular interest due to their pivotal roles in numerous biological processes and disorders. Variations in AA self-assembly not only affect protein structures and functions, but their non-covalent interactions such as hydrogen bonding, van der Waals forces, and π–π stacking, yield versatile assemblies vital in bio-inspired material fabrication. Tyrosine (Tyr), a non-essential aromatic amino acid, holds multifaceted significance in the body as a protein building block, neurotransmitter precursor, thyroid hormone contributor, and melanin synthesis regulator. The proficiency of Cold Atmospheric Plasma (CAP) in generating a spectrum of reactive oxygen and nitrogen species has spurred innovative research avenues in the studies of biomolecular components, including its potential for targeted cancer cell ablation and biomolecule modification. In this work, we have assessed the chemical as well as the structural changes in Tyrosine-derived self-assembled structures arising from the CAP-induced reactive species. For a comprehensive understanding of the mechanism, different treatment times, feed gases, and the role of solvent acidification are compared using various spectroscopic and microscopic techniques. LC-ESI-QQQ mass spectra unveiled the emergence of oxygenated and nitro derivatives of L-tyrosine following its interaction with CAP-derived ROS/RNS. SEM and TEM images demonstrated an enhanced surface size of self-assembled structures and the formation of novel nanomaterial-shaped assemblies following CAP treatment. Overall, this study aims to explore CAP's interaction with a single-amino acid, hypothesizing the creation of novel supramolecular structures and scrutinizing CAP-instigated transformations in L-tyrosine self-assembled structures, potentially advancing biomimetic-attributed nanomaterial fabrication which might present a novel frontier in the field of designing functional biomaterials.

1. Introduction

Cold atmospheric plasma (CAP) has demonstrated its efficacy in numerous industrial applications. Among these, its notable success has been in the biomedical sector, where it has showcased its potential in diverse areas such as oncology,[1,2] wound healing,[3,4] dermatology,[5,6] cosmetics, sterilization, disinfection,[7–9] dentistry,[3,10,11] and much more. This success has stimulated the emergence of a new field of study, known as plasma medicine.[2,12–16] Given CAP's capability to generate a wide array of reactive oxygen and nitrogen species, its effectiveness in interacting with biomolecules has led to inspiring innovative research opportunities, demonstrating its potential in selectively killing cancerous cells as well as modifying biomolecules such as proteins,[17–19] enzymes[20–22] and lipids.[22–24] With the hypothesis that the interaction between CAP and these biomolecules could lead to chemical modifications and the creation of novel supramolecular structures, our objective was to explore how CAP influences the self-assembly of small biomolecules that have the potential to form biomimetic materials, thereby introducing a new avenue for the development of biomaterials derived from CAP.

Self-assembly of biological macromolecules holds paramount importance in understanding the behaviour of biomolecules, especially proteins. In this regard, amino acids (AAs), which serve as the essential building blocks of proteins, hold a pivotal position where any alterations in the self-assembly

---

[a] *Physical Sciences Division, Institute of Advanced Study in Science and Technology, (An Autonomous Institute Under DST, Govt. of India), Vigyan Path, Paschim Boragaon, Garchuk, Guwahati, Assam 781035, India. E-mail: kamatchi.sankaran@gmail.com*

[b] *Academy of Scientific and Innovative Research (AcSIR), Campus Postal Staff College Area, Sector 19, Kamla Nehru Nagar, Ghaziabad 201002, Uttar Pradesh, India*

[c] *Department of Medical Device, National Institute of Pharmaceutical Education and Research, SilaKatamur (Halugurisuk), P.O.: Changsari, Dist: Kamrup, Guwahati, Assam-781101, India*

[d] *Department of Pharmaceutical Analysis, National Institute of Pharmaceutical Education and Research, SilaKatamur (Halugurisuk), P.O.: Changsari, Dist: Kamrup, Guwahati, Assam-781101, India*

† Electronic supplementary information (ESI) available. See DOI: https://doi.org/10.1039/d4ra01891e

process can have a profound impact on the functions and structures of proteins. Furthermore, the self-assembly of amino acids, primarily driven by many non-covalent interactions, such as hydrogen bonding, van der Waals forces, π–π stacking, *etc.* leads to the creation of diverse structures with applications in biomaterial formation. Consequently, a lot of research is gaining prominence on the self-assembly of amino acids and peptides, particularly for the development of nanostructures utilized in drug delivery, nanotechnology, biosensors, *etc*[25–30]. Aromatic amino acids have especially garnered the focus of researchers because of their involvement in many biological pathways and disorders, including neurodegenerative disorders, such as alzheimer's and phenylketonuria.[31] The aggregation of peptides and proteins involving aromatic amino acids is considered to be a cause of the formation, acceleration, and stabilization of ordered β-amyloid fibrils,[28,31,32] responsible for these disorders. Tyrosine (Tyr) is one such aromatic amino acid, having multi-functional roles in many important biological pathways of a living organism.[28,31] It functions not only as a building block of proteins but also as a precursor of several neurotransmitters (dopamine, epinephrine, norepinephrine)[33] and is also a key component in the synthesis of thyroid hormones (thyroxin, triiodothyronine).[34] It also holds a vital role as a melanin precursor as, during melanogenesis, the production of L-Dopa and Dopaquinone from Tyrosine is a rate-limiting step that further determines the synthesis of melanin. Tyr is known to form self-assembled structures in an aqueous medium and is utilized in the field of tissue engineering and the creation of biomimetic materials, especially due to its unique properties and ability to mimic natural extracellular matrix (ECM) components, thus enhancing the properties of biomaterial.[28,31,35–37] Existing studies on the fabrication of functional biomaterials have utilized methods like solvent-induced fabrication, adsorption on a metal substrate,[38,39] concentration variation[28] and enzymatic polymerization.[40,41] However, all these techniques involve the complexity of different solvents and chemicals, with some demanding precise temperature,[39] hence limiting the control over the fabrication process. The exploration of CAP in modifying self-assembled structures has not been studied extensively and remains an unchartered territory. The propensity of aromatic amino acids and peptides to self-assemble suggests that the aromatic residue is responsible for forming several nanostructures.[35,42] Several oxidation reactions regulate the ROS-sensitive moieties of the amino acids, thus regulating the hydrophobicity or conjugation of amino acids, consequently modifying their tendency to aggregate.[43–45] Thus, we propose that a controlled release of the RONS *via* cold atmospheric plasma can be utilized to regulate the self-assembly process of the biomolecule with potential use in tissue engineering, biosensing or imaging, and drug delivery.[43,44,46,47] The assessment of CAP-induced alterations of Tyr-inspired self-assembled structures is still a novel concept and might provide a new avenue for the controlled fabrication of bio-mimetic functional materials. In this work, we have investigated CAP-induced self-assembled structures of L-tyrosine using different chemical as well as morphological studies for their potential role in the designing and fabrication of bio-mimicking functional biomaterials. We have proceeded to assess whether comparable effects manifest in both buffered and non-buffered solutions, thereby elucidating the impact of CAP-induced acidification.

The 2-D chemical structure of L-tyrosine is shown in Fig. 1. The molecular formula is given by $C_9H_{11}NO_3$. L-tyrosine is a non-essential amino acid consisting of carboxylic acid on one side and the amide group on the other with a side chain consisting of an aromatic phenyl group. It is an optically active form of tyrosine, which is derived from phenylalanine and is a precursor of epinephrine, thyroid hormone, and melanin.

2. Materials and methods

2.1 Sample preparation

L-Tyrosine (extra pure) was purchased from Sigma and dispersed in Milli-Q water with 1 mM (0.182 mg mL^{-1}) concentration. The solution was kept on a magnetic stirrer (300 rpm) for 2 hours for proper dissolution at room temperature (25 °C). For plasma treatment, 5 mL of the dissolved sample was kept on a Petri dish under the plasma jet nozzle, treated with different gases at different times, and then taken for further characterization. All characterizations were done in aqueous medium.

2.2 Experimental setup of plasma jet

The experimental setup consists of an indigenously developed atmospheric plasma jet whose details are mentioned in the previous works.[48] The schematic diagram of the experimental setup and the photograph of the lab-developed plasma jet setup are given in Fig. 2. In summary, the arrangement comprises a glass tube with a 3 mm inner diameter and a 7 mm outer diameter. The live electrode inserted inside the glass tube is made of stainless steel and is 1 mm wide. The outer surface of the glass tube was wrapped by an aluminium strip around the end of the tube which serves as the ground electrode. The distance between the tip of the nozzle and the sample was kept at 5 mm throughout the experiment. An HV power supply (Ionics Power Solutions Pvt. Ltd) was used to supply a high voltage of 5–6 kV and a frequency of 25 kHz. Helium and an admixture of helium and compressed air act as the feed gas for producing plasma whose flow rate was maintained at a constant 1–1.5 SLM (standard litre per minute) for helium. For helium air, additional air with airflow of around 0.2 SLM was added to 1 SLM helium to maintain a stable plasma. The flow rate was gauged using a variable flowmeter (Cole Palmer), and the plasma generated within the tube was expelled into the ambient

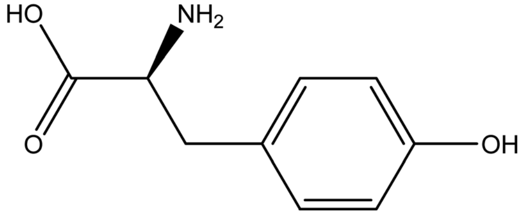

Fig. 1 2-D chemical structure of L-tyrosine amino acid.

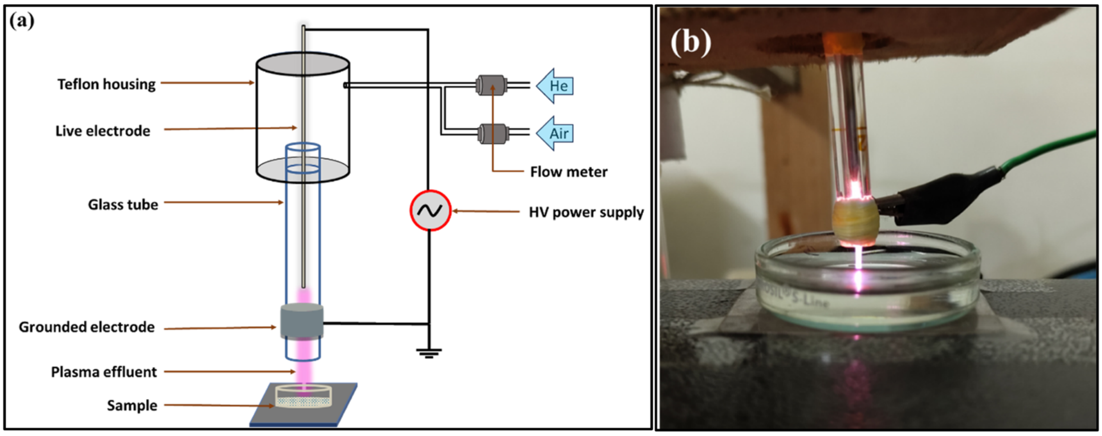

Fig. 2 Schematic diagram of the experimental setup (a); photograph of the lab-developed plasma jet setup (b).

air alongside the gas flow. The plasma formed between the electrodes is characterized by the OES spectra done in previous work from our lab.[48] Proper care was taken to minimize environmental variations during CAP treatment.

2.3 pH analysis of plasma-treated samples in aqueous and buffer solutions

The sample's pH was evaluated before and after the plasma treatment using a pH meter (Labtronics) at room temperature. To compare and elucidate the effect on the buffered solution, L-tyrosine (1 mM) was dissolved in a potassium phosphate buffer (100 mM) solution, with pH adjusted to 7.5. The pH of the aqueous and the buffered solutions of L-tyrosine were then compared before and after the plasma treatment.

2.4 Spectroscopic analysis of the sample

The UV-visible analysis was performed using a UV-1800-Shimadzu spectrophotometer. The photoluminescence of samples was recorded at the excitation wavelength of 275 nm using Cary Agilent, FP-8300. To detect any changes in the functional groups, the samples were first air-dried using a lyophilizer (Labonco) to remove any excess moisture content before being analysed for FTIR using the PerkinElmer spectrum. All the spectroscopic analyses were repeated in triplicates.

2.5 DLS and zeta potential analysis

For gauging the hydrodynamic size, the Polydispersity index and the formation of potential aggregates, the dynamic light scattering (DLS) and zeta potential of the treated and untreated samples were measured using the Zeta sizer (Malvern Analytical-NanoZS90). The measurements were repeated in triplicates and the average values were plotted and reported.

2.6 Liquid chromatography triple quadrupole (LC-QQQ) mass-spectroscopy analysis

We analysed the samples for changes in their masses after different times and feed gases of plasma treatment. The MS scan was conducted utilizing an Agilent 1290 Infinity II high-performance liquid chromatography system, coupled with an Agilent 6495C triple quadrupole mass spectrometer operating in both positive and negative ionization modes *via* electrospray ionization. The sample scan was performed in union with the solvent system used for analysis was isocratic. The optimized parameters under standard operating conditions for the MS scans included a gas source temperature of 300 °C, a drying gas rate of 5 L min^{-1}, a nebulizer pressure of 45 psi, a spray voltage of ±3500 V, and a sheath gas temperature of 250 °C. The sheath gas flow was set at 11 L min^{-1}. MS studies were conducted in positive and negative ionization modes with mass-to-charge ratio (m/z) ranges of 50 to 1000. For data recording in both positive and negative modes, scan rates of 1.0 scans per second were employed. The mobile phase consisted of 0.1% formic acid in a mixture of water and acetonitrile (50 : 50 v/v).

2.7 Morphological and structural changes of the samples

To comprehend the impact of CAP on the self-assembly process of tyrosine, various microscopy techniques, such as AFM, SEM, and TEM were employed. AFM studies were done on freshly prepared liquid samples of tyrosine, coated on glass slides using the drop-cast technique, and kept for overnight drying at room temperature. The experiments were performed using AFM-NTEGRA, NTMDT in contact mode. The AFM studies were followed by electron microscopy techniques like SEM and TEM analysis. For SEM analysis, the samples were prepared by dropping 100 μL of diluted sample on a glass slide and left for overnight drying. The dried samples were followed by gold-coating using a plasma sputtering technique. The model used for the SEM analysis was SIGMA-VP FESEM, ZEISS. For TEM analysis, the sample was diluted to 100 μM and then a small drop was cast upon the copper grid and left for vacuum drying overnight. The TEM analysis was done using JEM-2100, JEOL.

3. Results and discussions

3.1 Spectroscopic analysis

Fig. 3(a and b) shows the UV absorption of samples before and after treatment with helium and He–air cold plasma. The

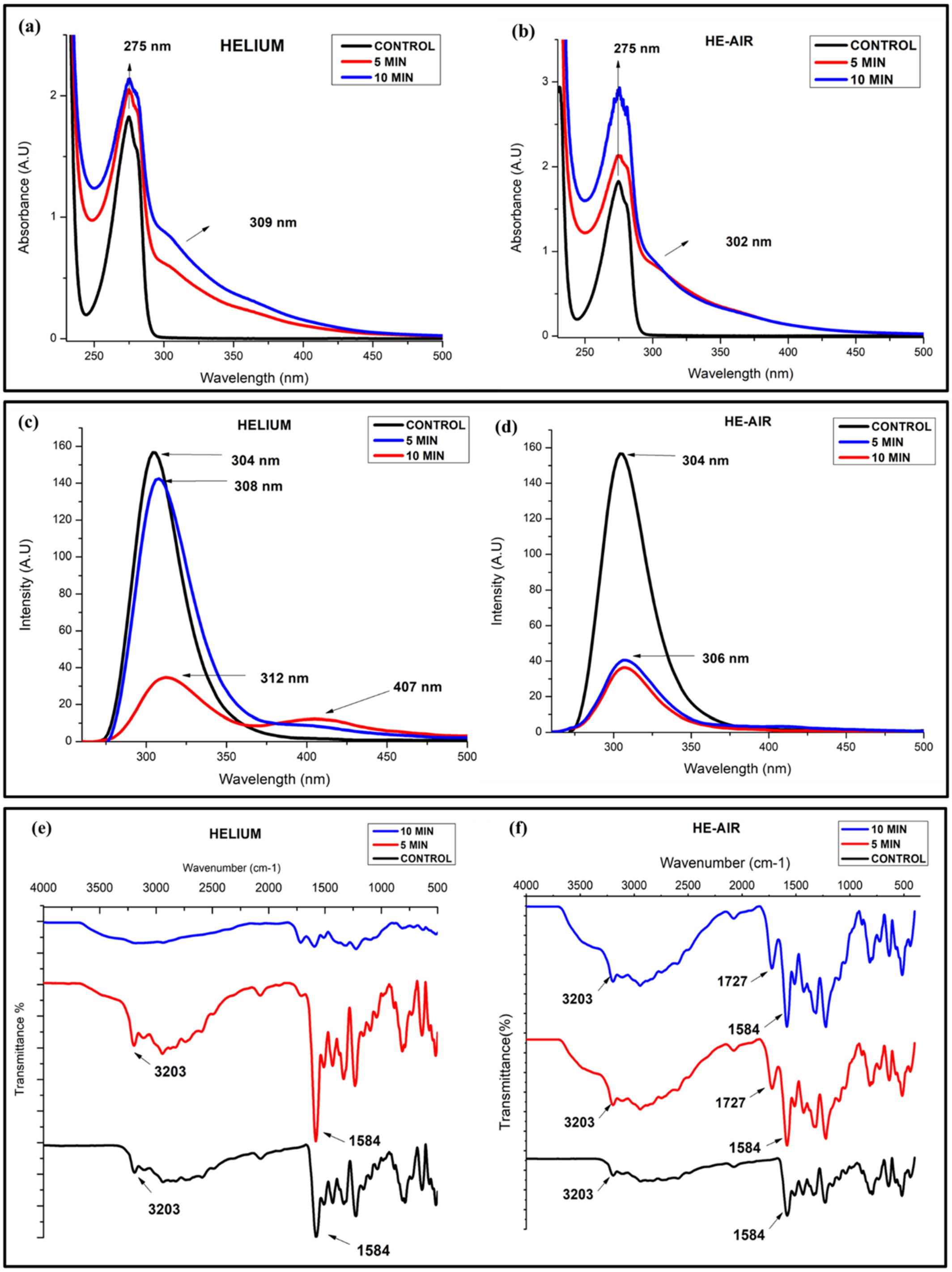

Fig. 3 UV-visible spectra (a and b), fluorescence quenching (c and d) and FTIR spectra of L-tyrosine (1 mM) with helium and He–air treated cold plasma (e and f).

maximum absorbance peak of tyrosine is observed at $\lambda_{\max} = 275$ nm for the untreated sample, corresponding mainly to the n → π* transition to its carboxylic group.[49] The figure shows that the plasma-treated samples show an increase in the absorbance intensity of the peak without any significant shift in the peak with a shoulder peak at ∼302 nm. The increase in the absorbance could result from probable aggregations in the samples after the plasma treatment.[50] The appearance of a new peak in the UV-visible spectra of CAP-treated tyrosine suggests that the treatment has induced significant changes in the molecular structure, composition, or environment of the tyrosine molecules, leading to the emergence of distinct optical features in the spectra (Fig. 3(a and b)). The appearance of a new emission peak is also observed in the fluorescence studies where the

10 min treated sample in helium treated samples highlights another smaller peak at around 407 nm apart from the characteristic peak of tyrosine at 304 nm (Fig. 3(c)). This new peak might indicate towards the formation of a new tyrosine-based complex when it undergoes a redox process after interacting with the CAP-induced radicals. In addition to that, there is a noteworthy quenching of the fluorescence peak in the CAP-treated samples (Fig. 3(c and d)). The quenching process can occur due to various reasons attributable to the influence of the different solvent conditions, out of which ionization of its phenolic group, quenching of fluorescence by its own dissociated carboxyl group, and the effect of its solvent's pH are some of the well-known mechanisms.[51]

Since we have prepared our samples in water, there is a huge chance that the modifications in the spectra might be attributed to the ionization of the Tyr side chain due to interaction with its environment, which could be a result of the decreasing pH of the solvent.[49] To check whether this variation in absorbance is due to the acidification of the solvent, we performed the same analysis using an acidified solution of tyrosine (controlled study). The results (Fig. S1(a)†) showed that there was no change in the absorbance intensity of the acidified tyrosine in the particular pH range (pH-2.7). The decrease in fluorescence intensity of Tyr is also visible in the controlled studies (Fig. S1(b)†). It is understood that the decrease in fluorescence intensity of Tyr due to a pH below 4 is attributable to the appearance of its non-ionized carboxyl group.[51,52] However, in addition to this, the peaks are also slightly shifted towards a longer wavelength in the case of helium–plasma treated samples, The red shift in the Tyr chromophore may be due to hydrogen bonded to the carboxyl group or other good proton acceptors,[51] whereas no shifting or emergence of any new peak is observed in the controlled study of the sample (Fig. S1(b)†). Thus, the mechanistic action of radicals coming out of the cold plasma has affected the optical properties of tyrosine through substantial alterations in the molecular structure, composition, or surrounding environment of the tyrosine molecules resulting probably from the ionization of the phenol group and by inducing charges to the nearby amino and carboxyl groups.[27]

The presence of any functional group and the related modifications are tested using the infrared spectroscopy technique. Fig. 3(e and f) shows a comparison between the untreated and treated samples of helium and He–air plasma. The peak significant at 3203 cm^{-1} is perhaps due to the NH stretching and OH group present in the amino acid while several peaks in the range 3000–3200 cm^{-1} correspond to the CH stretching vibrations of the aromatic group present in the compound. The 1584 cm^{-1} peak seen in the untreated samples' spectra characterizes the C=N stretching vibrations.[53] After the samples were treated with cold plasma, the helium 10 min treated sample resulted in the merging of the peaks, resulting in a broad and much weaker intensity peak at around 2700–3200 cm^{-1}. The merging of the peaks and emergence of a broad peak at around 3200 might signify that the 10 min helium-treated sample has a much higher OH content, probably due to the oxidation of the phenolic group of the tyrosine.[54] A similar merging is also seen for other peaks at a lower wavenumber (less than 1700 cm^{-1}). The merging of the peak might signify an alteration in the bonding of the molecules among themselves, or with another neighbouring molecule present, especially due to the changes in the solvent conditions. In the case of helium–air plasma, both 5 min and 10 min treated samples show a new peak at 1727 cm^{-1} which is not seen in the untreated samples. The peak corresponds to the presence of the C=O bond of aldehydes or ketones, observed only in the treated samples, showing an enhanced emergence of carbonyl groups in the CAP-treated compounds. It is interesting to know that neither of these effects were visible in the controlled study of the sample and the FTIR spectra of acidified tyrosine gave no observable modification in the spectra (Fig. S1(c)†). Thus, the controlled study underscores that the outcomes outlined in this section are a result of an interaction of CAP-generated reactive species with the tyrosine residue.

3.2 Liquid chromatography-ESI (QQQ) mass-spectroscopic analysis

To investigate the findings of the spectroscopic analysis and examine the chemical modifications arising from the ROS/RNS, the mass spectra of the untreated and the CAP-treated samples of an aqueous solution of tyrosine were done using the LC-ESI-triple quadrupole mass spectroscopy (QQQ-MS).

The mass spectra of the protonated control samples of tyrosine, $(\text{Tyr})\text{H}^+$ *i.e.*, samples before the plasma treatment and labeled L-Tyr in Fig. 4(a), are detected at the *m*/*z* value of 182.0 $(\text{M} + \text{H}^+)$. The elemental composition of the parent compound of tyrosine is observed as $C_9H_{11}NO_3$. As the sample ran in the scan mode, the spectra showed many other peaks in the mass spectra of control samples at the *m*/*z* value of 182.0, 202.1, and 227.1, out of which, the 182.0 *m*/*z* peak corresponds to the protonated tyrosine. The other peaks are considered to be arising from the other compounds present in the instrument, categorized as background noise.

Following the CAP treatment, few distinct peaks were observed in the He and He–air treated samples, indicating the presence of various oxidation and nitration products. The aromatic ring in tyrosine is known to undergo diverse reactions, including hydroxylation, nitration, and dehydrogenation.[55–57] By carefully comparing all the peaks present in the control and plasma-treated samples' spectra, we evaluated only those major peaks that were not present in the control samples' spectra. These were presumed to have arisen due to the chemical modifications induced by the reactive species present from CAP and might have an important effect on the structural and morphological changes, thereby altering the self-assembly process.

Five major peaks that were not present in control samples were identified with mass values 197.9 *m*/*z*, 213.0 *m*/*z*, 253.0 *m*/*z*, 255.0 *m*/*z*, and 274.2 *m*/*z*.

The first peak distinct peak is given by the *m*/*z* value of 197.9, which is probably because of the mono-oxidation of protonated tyrosine $[(\text{Tyr} + \text{O})\ \text{H}^+]$ labeled as L-Tyr + O along with the schematic chemical structure in Fig. 4(b). This peak is present in all other 4 plasma-treated samples having a similar intensity

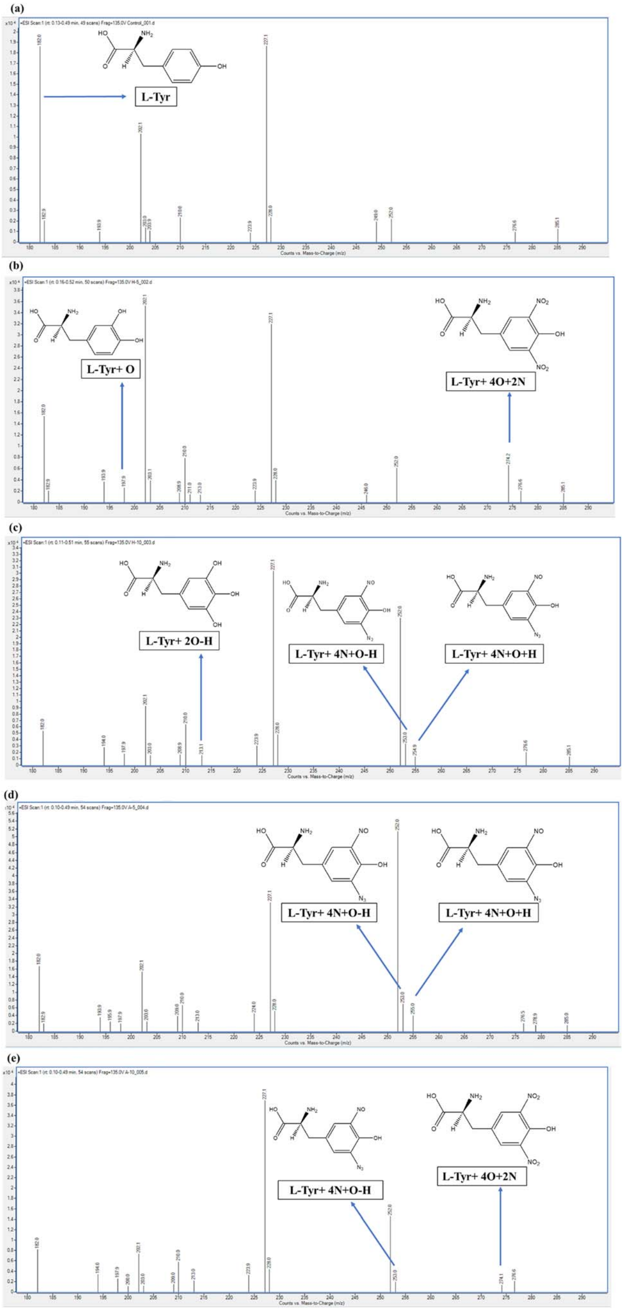

Fig. 4 LC-QQQ-mass spectra of the aqueous solution of protonated tyrosine sample [(Tyr)H$^+$] (a), helium-treated L-tyrosine samples at 5 min and 10 min (b and c) and He–air treated L-Tyr samples at 5 min and 10 min (d and e).

[Fig. 4(b–e)]. The elemental composition and structure of the predictive compound are given as $C_9H_{11}NO_4$ and shown in the respective figure. Another distinctive peak present in all 4 plasma-treated samples is identified at an *m*/*z* value of 213.0. The elemental composition for the same is presumed to be $C_9H_{10}NO_5$, which is a di-oxidized protonated tyrosine after the dehydrogenation and is labeled as L-Tyr + 2O–H and the schematic chemical structure drawn in Fig. 4(c).

The other three additional products, distinguishable from the control sample, exemplify the nitration of the parent compound. These are identified at *m*/*z* values of 253.0, 255.0, and 274.2 and the peaks are indicated and labeled in Fig. 4. The 253.0 *m*/*z* peak corresponding to L-Tyr + 4N + O–H is present in He 10 min and He–air 5 and 10 min samples, while the 255.0 *m*/*z* peak, corresponding to L-Tyr + 4N + O + H is observed only in the He 10 and air 5 min samples. The 274.2 *m*/*z* peak which corresponds to L-Tyr + 4O + 2N is only seen significantly in He 5 min and less intensely in He–air 10 min sample. The chemical composition for the three predictive products is $C_9H_{10}N_5O_4$, $C_9H_{12}N_5O_4$, and $C_9H_{11}N_3O_7$ respectively.

The analysis showed exactly how the oxidation of tyrosine takes place by the hydroxylation of the phenolic group, in addition to the nitration and dehydrogenation of the amino acid after the plasma-treated samples at different times and different feed gases. These structural changes corroborate the aforesaid discussion regarding chemical changes. For example, the addition of the Nitro group in the phenolic group tyrosine is known to be responsible for the decrease in the pK_a value of the hydroxyl group leading to deprotonation. This deprotonation of the phenolic hydroxyl group is also associated with the changes in the absorption spectra of tyrosine,[58] which possibly explains the increase in the absorption intensity.

3.3 Morphological studies

We further wanted to examine the size and morphology of CAP-treated samples as a result of potential alterations in its self-assembly process, following the aforementioned chemical modifications. The changes in the self-assembled structures are expected since oxidative and nitrative modifications can disrupt the hydrogen bonding and π–π interactions critical for tyrosine self-assembly, leading to altered aggregation kinetics, morphology, and stability of the resulting structures.

We conducted a particle size assessment using Dynamic Light Scattering (DLS). DLS is a method that utilizes the scattering of particles in a solution to estimate their size. While DLS offers a broad spectrum of particle sizes in the solution, it may not precisely determine the exact particle size. Nevertheless, it effectively offers insights into changes in particle size and the detection of agglomerated particles.[59] As illustrated in Fig. S3(b),† the DLS analysis indicates a greater particle size, suggesting the potential agglomeration of particles, or a completely different structure, following the CAP treatment. To validate and check the formation of the CAP-treated tyrosine samples, the surface morphology of the samples was studied using various microscopic techniques.

Fig. 5 shows the AFM images showcasing the self-assembled structures of L-tyrosine and the modifications of these structures after the CAP treatment. The control sample of Tyr in an aqueous medium showed its characteristics of self-assembled strip-like, nanoribbon-shaped structures, with cross-sectional thickness in the range of 500–700 nm as analysed by ImageJ software, which is in agreement with already available literature.[28,36] These structures were pointed towards the tips, thus giving it a needle-liked shape. Self-assembled structures of tyrosine were fragmented after CAP treatment and small agglomerated nano-sized particles are seen in the images. In

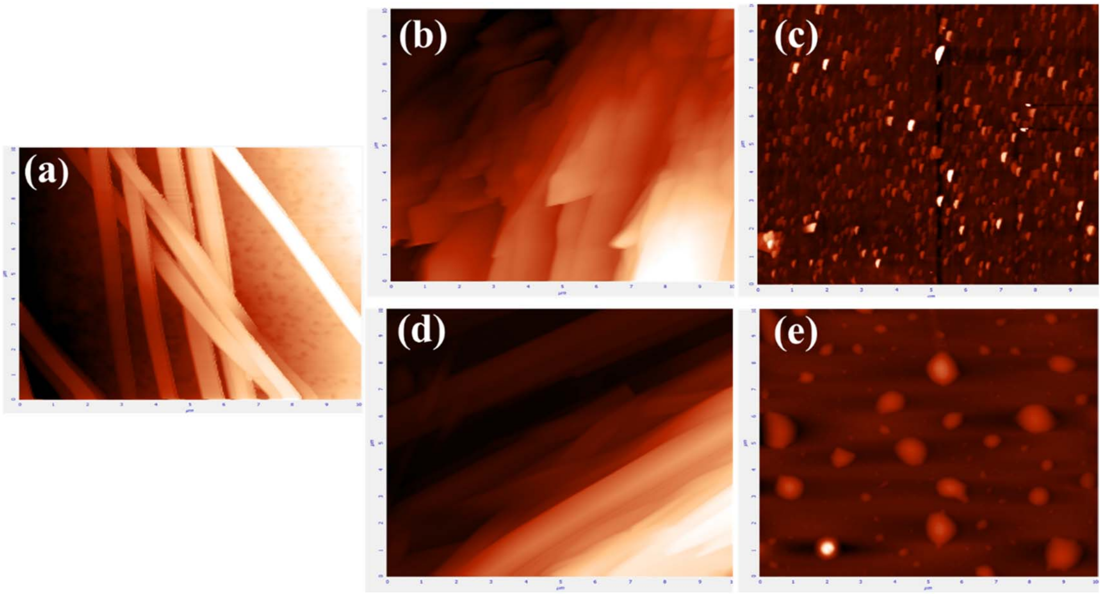

Fig. 5 AFM images of tyrosine control samples (a) and samples treated with helium (b and c) and He–air plasma (d and e) for 5 and 10 min respectively.

5 min samples, the nano-ribbons were seen to be distorted from their shape while the 10 min samples observed the complete fragmentation of structures [Fig. 5(b and c)], and showed the formation of particle-like structures. This pattern was reiterated in the case of He–air [Fig. 5(d and e)], but in this case, the particles showed a much uniform agglomeration of particles in 10 min treatment, having a spherical structure of diameter ranging from a minimum of 100 nm to a maximum of 1 μm. AFM imaging provided little information about the structural changes in the self-assembled structures of L-tyrosine but gave a significant hint in predicting the formation of different, probably novel structures. To further probe these structural formations, electron microscopy techniques such as SEM and TEM were used.

SEM provides a very good technique to visualize the surface morphology of the samples giving a 3D imaging. The nano-ribbon-shaped structures were also observed in the control samples of SEM images [Fig. 6(a)]. The treated samples of He and He–air for 5 and 10 min are shown subsequently in Fig. 6(b–e). For the He 5 min treated samples, the ribbon-shaped structures are seen to be a little widened, without any change in the shape. The 10 min-treated samples showed complete defragmentation of the fiber-liked self-assembled tyrosine and exhibited a unique crystalline-flaky structure, giving a completely different morphology with sharp edges and a broader surface area. The size of each leaflet in the structure has a much greater surface area as can be seen in a higher magnification image [Fig. S2†]. In the case of He–air, the 5 minutes treatment was enough to form the complete accretion of particles. These particles show much sharper-edges and higher surface area, while the 10 min sample shows the formation of clustered particles. This indicates that the reactive species of two different feed gases result in a completely different interaction among the Tyr group, giving rise to different assemblies at different treatment times. The formation of larger aggregates after CAP treatment was also reflected in the zeta potential measurements where the zeta potential of the plasma-treated samples is observed to be shifting toward zero or a lesser negative value. (Fig. S3(a)†). The magnitude of the zeta potential reflects the electrostatic repulsion between similar particles, reflecting the stability of particles. Thus, when the zeta potential approaches zero, typically known as the isoelectric point,[41] it suggests a heightened likelihood of coagulation. These changes are potentially due to the alteration of charge distribution due to plasma-generated species interacting with the surface functional groups of tyrosine. It can also be due to alterations in pH, since pH can influence the ionization state of functional groups on tyrosine molecules, impacting their overall charge and zeta potential. The structural changes might be entirely varied in the case of buffered solvents, as the solvent properties would not affect the amino acid side chain interaction with the reactive species. Such CAP-instigated structures propose a great potential to be used for drug delivery using nanoparticles due to an enhanced surface area and edgy-leaf-like structures which is an essential attribute in the application of nano biomaterials owing to its higher binding efficiency and leading to an enhanced interaction with the biological environment, such as allowing better Blood–brain barrier (BBB) crossing in the case of Neurotherapy.[29,60]

Transmission Electron Microscopy (TEM) analysis revealed the formation of nanoparticle-sized structures by using a focused beam of electrons through the sample and giving a projected 2D image of its internal structure. Fig. 7 shows the internal structure of control and CAP-treated tyrosine, as seen through TEM analysis. The self-assembled fibril structures of tyrosine are deformed after treating them with plasma, moving

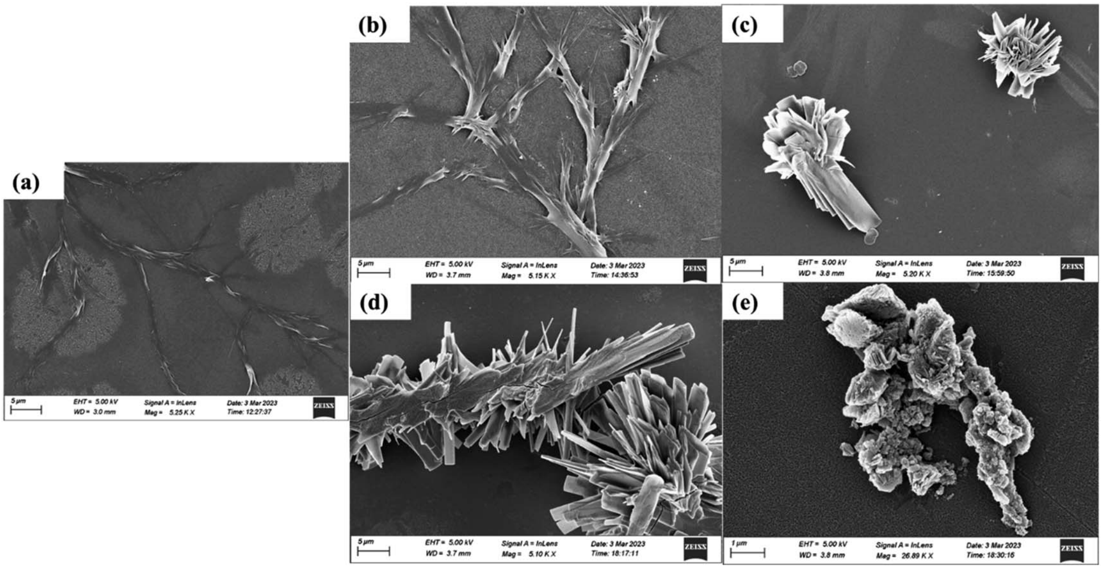

Fig. 6 SEM of images of control L-tyrosine (a) and L-tyrosine treated with helium (b and c) and He–air plasma (d and e) for 5 and 10 min respectively.

towards the formation of grain-like morphological formations. These formations, particularly evident in the helium 10 min sample (Fig. 7(c)), manifest as an assembly of nanoparticles distributed uniformly in a colonial pattern, with each particle having a diameter of around 80 nm, as analysed by ImageJ software. A similar kind of particle formation is visible in He–air plasma treatment [Fig. 7(d and e)]. The formation of similar geometry particles can be substantiated in the He–air-10 min case, with particles seen as darker dotted structures. The formation of such granular structures in the nanometre range can prove to be a novel method of fabricating supramolecular structures, by regulating the self-assembled structures of existing biomimetic functional materials based on their requirement.

3.4 Physio-chemical analysis of samples

To delve into the mechanism behind these modifications, we conducted a pH analysis of the CAP-treated samples Table 1 showed that the pH of L-tyrosine was 6.48 before the treatment, however after treating it with CAP, the pH changed to 3.51 in the

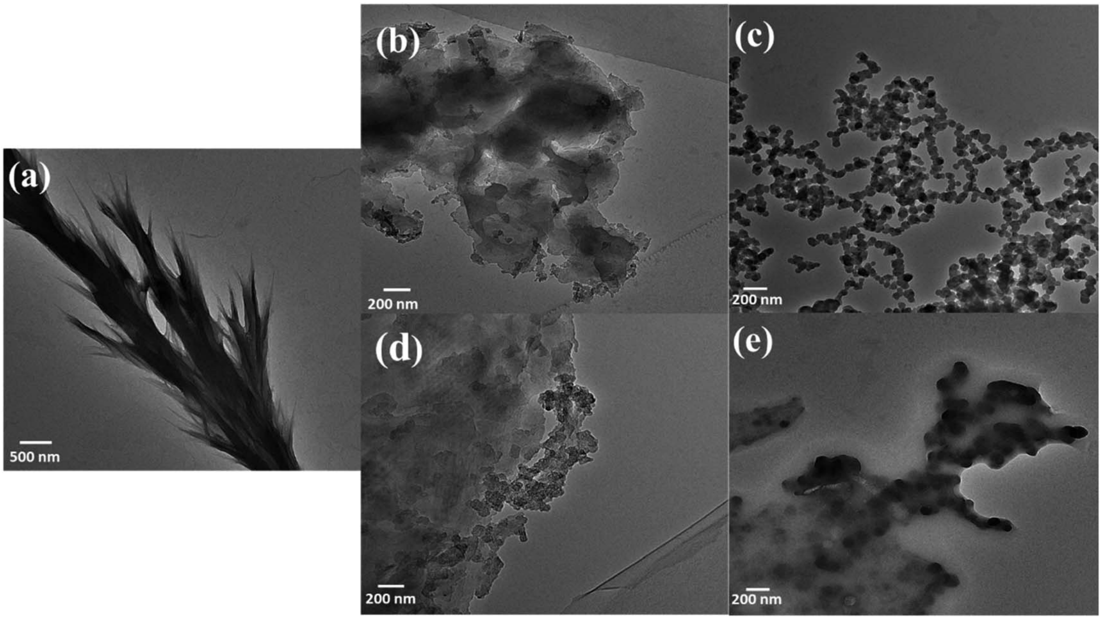

Fig. 7 TEM images of control L-tyrosine (a) and L-tyrosine treated with He-treated (b and c) and He–air treated (d and e) plasma for 5 and 10 min respectively.

5 min sample and 3.14 in the 10 min sample (Table 1), in case of helium, indicating the acidification of the amino acids caused by CAP treatment, in accord with the other reported results.[61] Further, the samples were also prepared using phosphate-buffered solutions, and the pH was adjusted to 7.5. In the case of buffered solutions, it was noticed that the pH remained consistent following plasma treatment, with only a marginal decrease in the values. (Table S1†). Thus, acidification was clearly witnessed more in the aqueous medium than in the buffer case. Further, a longer duration of CAP treatment shows more substantial acidification, demonstrating the role of the concentration of the plasma-induced reactive species in lowering the pH. Thus, the evaluation of CAP-induced acidification in the self-assembly process and chemical structure alteration of tyrosine becomes crucial.

The modifications caused by the CAP are all attributed to the reactive species (hydrogen peroxide, nitrate, nitrite superoxide, peroxynitrite nitric oxide, *etc*) existing within it. Thus, to enumerate the RONS present, we calculated the presence of different ROS and RNS using the quantification method mentioned in the literature.[48,62,63] Briefly, H_2O_2 in plasma-treated water was measured using a red fluorescence hydrogen peroxide kit (purchased from Sigma-Aldrich) and NO_2/NO_3 was quantified using a chemical nitrate/nitrite colorimetric assay kit (Cayman). The widely used procedure of terephthalic acid (TA) was used to measure OH radicals. TA reacts with the OH radicals to give 2-hydroxyterephatalate (hTA) to give fluorescence at 425 nm. TA was dissolved in water (330 μM), treated with a cold plasma jet, and taken for fluorescence analysis with excitation at 312 nm and emission at 412 nm.

Table 2 shows the concentration of reactive species, such as hydrogen peroxide (H_2O_2), nitrate, and nitrite, produced in the medium after treating it with cold plasma. The rise in the concentration of reactive species over the treatment duration suggests that the generation of H_2O_2, OH, NO_2, and NO_3 from plasma could contribute to the previously discussed acidification of the solution. Many groups have already stated the reason for the cause of this acidification, suggesting that H_2O_2 (ref. 64 and 65) and reactive nitrogen species are responsible for this acidification, with NO_2 being the most common cause as it undergoes the hydrolysis process when in contact with an aqueous medium. The buffer, on the other hand, consumes the hydronium ions produced during this reaction.[61,65,66] These reactive species also influence the self-assembly process of the amino acid by reacting with its environment and giving rise to aggregation and distinct assembled structures, as observed.

Table 1 pH comparison of untreated (control) and CAP-treated samples in an aqueous medium

Feed gas	pH (control)	pH (5 min)	pH (10 min)
Helium	6.48	3.51	3.14
He–air	6.48	2.94	2.50

4. Comparison of the effects in buffered solution

The CAP produced reactive species in L-tyrosine and its comparison with the controlled studies in Section 3.1 revealed that acidification is not the only factor in the aforesaid chemical modification. To better understand the CAP-based mechanism, we checked whether the plasma reactive species leads to the same biophysical changes in a buffered solution. 1 mM of L-tyrosine was dissolved in PBS (7.5) and treated under CAP-jet using the same parameters as discussed above. The treated solution was then taken for spectroscopy and morphology analysis. As can be seen from Fig. 8(a and b), the UV-vis absorption of the untreated samples increases as plasma exposure time increases, indicating the possible aggregation of the particles with increasing treatment time. The trend of absorption increase is similar to the one in the water (non-buffered) solution. Thus, plasma reactive species indeed lead to possible aggregation of particles irrespective of the pH change. The fluorescence quenching after the CAP treatment is also visible in the buffered solution. However, the emergence of no new peaks is observed in this case. Further, the trend of this quenching is similar in both the feed gases, without any significant change (Fig. 8(c and d)), in contrast to what is observed in the water solution, signifying that the reactive species in a non-buffered solution interact differently with the sample. The FTIR spectra show that there is a widening of the 3200 cm^{-1} peak corresponding to the increase in the OH functional group, especially after the 10 minutes treatment of the feed gases. This kind of widening is also observed in the water solution, probably indicative of the increase in the OH functional group due to the tyrosine oxidation in the plasma-treated samples. Further, there is no new peak observed in the spectra, except for some merging of the peaks at 1136 cm^{-1} (Fig. 8(f)). From this, it is assumed that the CAP treatment in buffer alters the bonding of the molecules, without any substantial change in its chemical structure.

To check whether the CAP instigates a similar kind of self-assembled structure in the buffered solution, SEM and TEM were performed. The SEM images (Fig. 8(g)) showed the fibrillar structures of L-tyrosine in the untreated samples of almost the same morphology as in the water solution. Upon plasma treatment, the fibrillar structures of tyrosine are defragmented, and distinct self-assembled structures are formed, with smaller flower-like structures, with the petal size less than a micron. A similar kind of assembly is seen in both the feed gas without much variation (Fig. 8(h–k)). This is different than what is observed in the water solution, wherein we can see an increase in the sizes of the self-assembled structures through the SEM imaging. This is because the buffer, in this case, would prevent CAP-produced reactive species from interacting with the amino acid side chain resulting in different hydrogen-bonded complexes. The TEM imaging further indicates no uniform nanoparticle creation in the CAP-treated buffered solution (Fig. S4†). Further, no change in zeta potential and DLS size was observed, signifying that the zeta potential change in the water

Table 2 Quantification of reactive oxygen and nitrogen species for He and He–air-fed plasma

Feed gas/treatment time (min)	Hydroxyl radicals (μM)	H_2O_2 (μM)	Nitrate (NO_3^-) (μM)	Nitrite (NO_2^-) (μM)
He (5 min)	14.7 ± 0.9	571.82 ± 8.46	4.35 ± 0.34	7.39 ± 0.19
He (10 min)	12.9 ± 0.24	587.41 ± 8.79	8.13 ± 0.53	17.46 ± 0.21
He–air (5 min)	55.943 ± 0.088	90.609 ± 0.005	774.8 ± 0.13	19.95 ± 0.08
He–air (10 min)	43.363 ± 0.042	89.716 ± 0.006	1469.39 ± 0.50	10.55 ± 0.07

solution was probably as a result of an alteration in pH. In the case of the buffer, overall charge and zeta potential were constant since the buffer prevented any change in the ionization state of the tyrosine functional group.

The results in this section reveal that cold atmospheric plasma results in completely different kinds of structural alterations in buffered and non-buffered solutions. Also, it's worth noting that acidification alone doesn't fully explain the observed chemical changes, as demonstrated by the controlled studies (Fig. S1†). Hence, the collective influence of CAP-induced reactive species along with associated effects, such as solvent acidification, accounts for the changes observed in the chemical composition and self-assembled structures of CAP-treated L-tyrosine across different solutions. One possible

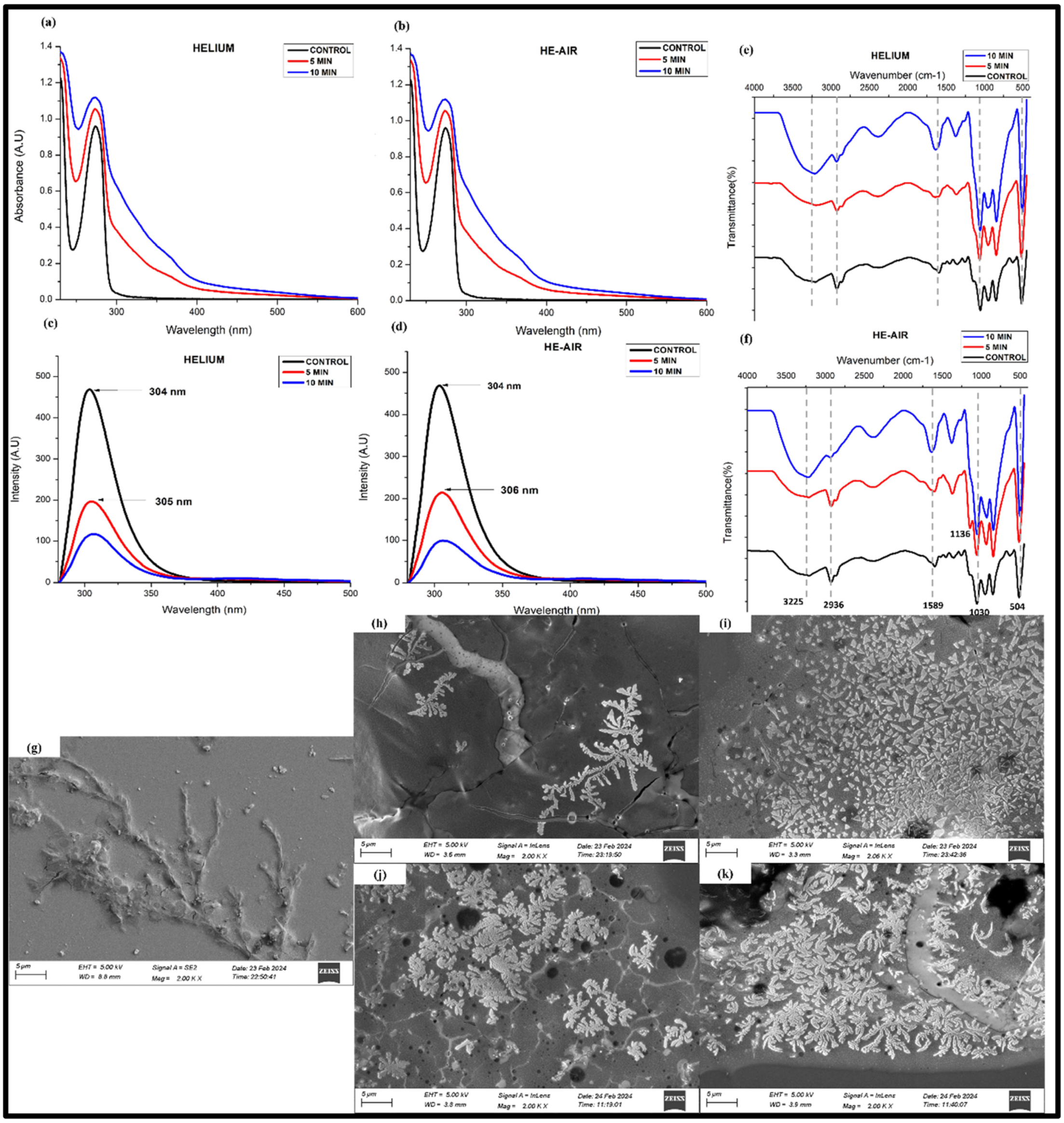

Fig. 8 UV-visible spectra (a and b), fluorescence spectra (c and d), FTIR spectra (e and f), and SEM images (g–k) of L-tyrosine treated with He-treated and He–air-treated plasma for 5 and 10 min respectively in PBS (7.5).

explanation for this is the pH dependence of several reactions influencing the plasma chemistry in the aqueous solution. For example, the decomposition of HNO_2 to dinitrogen oxide N_2O_3 only occurs in an acidic environment.[61,67] This N_2O_3 further leads to the formation of NO and NO_2, thus affecting the concentration of species and influencing their interactions within the solution. Similarly, the NO_2 conversion to NO and NO_2 after hydrolysis is affected by the amount of hydronium ions that are consumed in buffered solutions.

5. Conclusion

In this study, we have investigated the impact of cold atmospheric plasma on L-tyrosine-derived self-assemblies through various spectroscopic and morphological analyses. The findings reveal that CAP-generated RONS can effectively reorganize the self-assembled structures of L-tyrosine, thus forming distinct uniform nanoparticle-like structures. The spectroscopy and IR analyses add valuable information about changes in chemical structure post-CAP treatment. The LC-QQQ mass spectra predicted the chemical structure of newly formed compounds. Additionally, the microscopic techniques (SEM, AFM, TEM), reveal that interaction with the reactive species after CAP treatment leads to the creation of granular nanoparticle-like formations that can give an enhanced aspect ratio. By comparing the CAP-induced changes in buffered and acidified solutions, we concluded that a synergetic effect of all the reactive species produced from the plasma determines the chemical and biophysical changes in its structure as well as the self-assembly process.

Given L-tyrosine's capacity to mimic the biochemical and mechanical attributes of natural tissues, these newly created CAP-derived self-assembled structures can be modified and tuned according to the requirements, presenting promising avenues in nanomaterial-based drug delivery, biomaterial surface modification, and the development of functional biomaterials. However, comprehensive investigations into the mechanical, electrical, and optical properties of CAP-derived nanomaterials are essential to fully exploit their potential in tissue engineering, regenerative medicine, and biomaterial advancement.

Data availability

The data supporting the findings of this study are included within the article and the supplementary sheet provided.

Conflicts of interest

The authors declare no conflicts of interest.

Acknowledgements

Author KS thanks ICMR Project grant (File No. 17x(3)/Ad-hoc/19/2022-ITR dt. 23.12.2022) and DST-IASST, Guwahati In-house project grant. Author PB thanks IASST, DST, Govt. of India for the support for the Junior Research Fellowship. Author PB thanks AcSIR for their PhD registration.

References

1 D. Braný, D. Dvorská, E. Halašová and H. Škovierová, Cold Atmospheric Plasma: A Powerful Tool for Modern Medicine, *Int. J. Mol. Sci.*, 2020, **21**(8), 2932.
2 M. Laroussi, Plasma Medicine: A Brief Introduction, *Plasma*, 2018, **1**(1), 47–60.
3 B. Kleineidam, M. Nokhbehsaim, J. Deschner and G. Wahl, Effect of cold plasma on periodontal wound healing—an *in vitro* study, *Clin. Oral Invest.*, 2019, **23**(4), 1941–1950.
4 A. Schmidt, S. Bekeschus, K. Wende, B. Vollmar and T. von Woedtke, A cold plasma jet accelerates wound healing in a murine model of full-thickness skin wounds, *Exp. Dermatol.*, 2017, **26**(2), 156–162.
5 F. Tan, Y. Wang, S. Zhang, R. Shui and J. Chen, Plasma Dermatology: Skin Therapy Using Cold Atmospheric Plasma, *Front. Oncol.*, 2022, **12**.
6 L. Gan, J. Jiang, J. W. Duan, X. J. Z. Wu, S. Zhang, X. R. Duan, *et al.*, Cold atmospheric plasma applications in dermatology: A systematic review, *J. Biophot.*, 2021, **14**(3), e202000415.
7 S. J. Sung, J. B. Huh, M. J. Yun, B. M. W. Chang, C. M. Jeong and Y. C. Jeon, Sterilization effect of atmospheric pressure non-thermal air plasma on dental instruments, *J. Adv. Prosthodont.*, 2013, **5**(1), 2.
8 A. Sakudo, Y. Yagyu and T. Onodera, Disinfection and Sterilization Using Plasma Technology: Fundamentals and Future Perspectives for Biological Applications, *Int. J. Mol. Sci.*, 2019, **20**(20), 5216.
9 Reema, H. Bailung, K. Sankaranarayanan and D. Basumatary, Comparative Analysis of Direct Cold Atmospheric Plasma Treatment *vs.* Plasma Activated Water for the Deactivation of Omicron Variant of SARS-CoV-2, *Plasma Chem. Plasma Process.*, 2024, **44**, 1019–1030.
10 D. F. Kinane, P. G. Stathopoulou and P. N. Papapanou, Periodontal diseases, *Nat. Rev. Dis. Prim.*, 2017, **3**(1), 17038.
11 Y. D. Cho, K. H. Kim, Y. M. Lee, Y. Ku and Y. J. Seol, Periodontal Wound Healing and Tissue Regeneration: A Narrative Review, *Pharmaceuticals*, 2021, **14**(5), 456.
12 M. G. Kong, G. Kroesen, G. Morfill, T. Nosenko, T. Shimizu, J. van Dijk, *et al.*, Plasma medicine: an introductory review, *New J. Phys.*, 2009, **11**(11), 115012.
13 T. Bernhardt, M. L. Semmler, M. Schäfer, S. Bekeschus, S. Emmert and L. Boeckmann, Plasma Medicine: Applications of Cold Atmospheric Pressure Plasma in Dermatology, *Oxid. Med. Cell. Longev.*, 2019, **2019**, 1–10.
14 G. Fridman, G. Friedman, A. Gutsol, A. B. Shekhter, V. N. Vasilets and A. Fridman, Applied Plasma Medicine, *Plasma Processes Polym.*, 2008, **5**(6), 503–533.
15 M. Laroussi, Cold Plasma in Medicine and Healthcare: The New Frontier in Low Temperature Plasma Applications, *Front. Physiol.*, 2020, **8**, 74.
16 N. K. Kaushik, S. Bekeschus, H. Tanaka, A. Lin and E. H. Choi, Plasma Medicine Technologies, *Appl. Sci.*, 2021, **11**(10), 4584.

17 S. Sharma, H. Prabhakar and R. K. Singh, Atmospheric Cold Plasma-Induced Changes in Milk Proteins, *Food Bioprocess Technol.*, 2022, **15**(12), 2737–2748.

18 J. Wang, X. Zhou, J. Li, D. Pan and L. Du, Enhancing the functionalities of chickpea protein isolate through a combined strategy with pH-shifting and cold plasma treatment, *Innovat. Food Sci. Emerg. Technol.*, 2024, **93**, 103607.

19 K. C. Hsieh and Y. Ting, Atmospheric cold plasma reduces Ara h 1 antigenicity in roasted peanuts by altering the protein structure and amino acid profile, *Food Chem.*, 2024, **441**, 138115.

20 B. Murtaza, L. Wang, X. Li, M. K. Saleemi, M. Y. Nawaz, M. Li, *et al.*, Cold plasma: A success road to mycotoxins mitigation and food value edition, *Food Chem.*, 2024, **445**, 138378.

21 C. Zhou, Y. Hu, Y. Zhou, H. Yu, B. Li, W. Yang, *et al.*, Air and argon cold plasma effects on lipolytic enzymes inactivation, physicochemical properties and volatile profiles of lightly-milled rice, *Food Chem.*, 2024, **445**, 138699.

22 M. Gavahian, Y. H. Chu, A. Mousavi Khaneghah, F. J. Barba and N. N. Misra, A critical analysis of the cold plasma induced lipid oxidation in foods, *Trends Food Sci. Technol.*, 2018, **77**, 32–41.

23 J. Striesow, J. W. Lackmann, Z. Ni, S. Wenske, K. D. Weltmann, M. Fedorova, *et al.*, Oxidative modification of skin lipids by cold atmospheric plasma (CAP): A standardizable approach using RP-LC/MS2 and DI-ESI/MS2, *Chem. Phys. Lipids*, 2020, **226**, 104786.

24 N. Ravash, J. Hesari, E. Feizollahi, H. K. Dhaliwal and M. S. Roopesh, Valorization of Cold Plasma Technologies for Eliminating Biological and Chemical Food Hazards, *Food Eng. Rev.*, 2024, **16**(1), 22–58.

25 T. Dillon, Seroski GAH. Self-Assembled Peptide and Protein Nanofibers for Biomedical Applications, in *Biomedical Applications of Functionalized Nanomaterials*, 2018.

26 B. H. J. Gowda, S. Mohanto, A. Singh, A. Bhunia, M. A. Abdelgawad, S. Ghosh, *et al.*, Nanoparticle-based therapeutic approaches for wound healing: a review of the state-of-the-art, *Mater. Today Chem.*, 2023, **27**, 101319.

27 A. Mahmood and R. ASabour, *Fabrication of Nanostructures by Plasma Electrolysis*, Wiley-VCH, 2010, p. 251.

28 C. Ménard-Moyon, V. Venkatesh, K. V. Krishna, F. Bonachera, S. Verma and A. Bianco, Self-Assembly of Tyrosine into Controlled Supramolecular Nanostructures, *Chem.–Eur. J.*, 2015, **21**(33), 11681–11686.

29 T. Sahu, Y. K. Ratre, S. Chauhan, L. V. K. S. Bhaskar, M. P. Nair and H. K. Verma, Nanotechnology based drug delivery system: Current strategies and emerging therapeutic potential for medical science, *J. Drug Deliv. Sci. Technol.*, 2021, **63**, 102487.

30 M. Kaushik, R. Niranjan, R. Thangam, B. Madhan, V. Pandiyarasan, C. Ramachandran, *et al.*, Investigations on the antimicrobial activity and wound healing potential of ZnO nanoparticles, *Appl. Surf. Sci.*, 2019, **479**, 1169–1177.

31 S. Perween, B. Chandanshive, H. C. Kotamarthi and D. Khushalani, Single amino acid based self-assembled structure, *Soft Matter*, 2013, **9**(42), 10141.

32 Q. Wang, X. Yu, L. Li and J. Zheng, Inhibition of Amyloid-β Aggregation in Alzheimer's Disease, *Curr. Pharm. Des.*, 2014, **20**(8), 1223–1243.

33 S. C. Daubner, T. Le and S. Wang, Tyrosine hydroxylase and regulation of dopamine synthesis, *Arch. Biochem. Biophys.*, 2011, **508**(1), 1–12.

34 M. A. Shahid, M. A. Ashraf and S. Sharma, *Physiology, Thyroid Hormone*, 2023.

35 P. Singh, S. K. Brar, M. Bajaj, N. Narang, V. S. Mithu, O. P. Katare, *et al.*, Self-assembly of aromatic α-amino acids into amyloid inspired nano/micro scaled architects, *Mater. Sci. Eng. C*, 2017, **72**, 590–600.

36 R. Y. Adhikari and J. J. Pujols, Highly rigid & transparent supramolecular fibrils of tyrosine, *Nano Sel.*, 2022, **3**(9), 1314–1320.

37 S. Bera, B. Xue, P. Rehak, G. Jacoby, W. Ji, L. J. W. Shimon, *et al.*, Self-Assembly of Aromatic Amino Acid Enantiomers into Supramolecular Materials of High Rigidity, *ACS Nano*, 2020, **14**(2), 1694–1706.

38 F. R. Rahsepar, N. Moghimi and K. T. Leung, Surface-Mediated Hydrogen Bonding of Proteinogenic α-Amino Acids on Silicon, *Acc. Chem. Res.*, 2016, **49**(5), 942–951.

39 J. Reichert, A. Schiffrin, W. Auwärter, A. Weber-Bargioni, M. Marschall, M. Dell'Angela, *et al.*, l-Tyrosine on Ag(111): Universality of the Amino Acid 2D Zwitterionic Bonding Scheme?, *ACS Nano*, 2010, **4**(2), 1218–1226.

40 K. A. Marx, K. S. Alva and R. Sarma, Self-assembled micron-scale fibre structures are formed by amphiphilic decyl ester derivatives of the d- and l-tyrosine amino acids prior to and following enzymatic ring polymerization, *Mater. Sci. Eng. C*, 2000, **11**(2), 155–163.

41 K. A. Marx, S. OH and A. P. Angelopoulos, Gold Surface Adsorption Properties of the Enzymatically Polymerized Amphiphilic Decyl Ester of L-Tyrosine, *J. Macromol. Sci., Part A: Pure Appl.Chem.*, 2008, **45**(7), 503–510.

42 E. Gazit, A possible role for π-stacking in the self-assembly of amyloid fibrils, *Faseb. J.*, 2002, **16**(1), 77–83.

43 B. Hu, Z. Lian, Z. Zhou, L. Shi and Z. Yu, Reactive Oxygen Species-Responsive Adaptable Self-Assembly of Peptides toward Advanced Biomaterials, *ACS Appl. Bio Mater.*, 2020, **3**(9), 5529–5551.

44 N. Song, Z. Zhou, Y. Song, M. Li, X. Yu, B. Hu, *et al.*, In situ oxidation-regulated self-assembly of peptides into transformable scaffolds for cascade therapy, *Nano Today*, 2021, **38**, 101198.

45 N. Ma, Y. Li, H. Xu, Z. Wang and X. Zhang, Dual Redox Responsive Assemblies Formed from Diselenide Block Copolymers, *J. Am. Chem. Soc.*, 2010, **132**(2), 442–443.

46 X. Du, J. Zhou, J. Shi and B. Xu, Supramolecular Hydrogelators and Hydrogels: From Soft Matter to Molecular Biomaterials, *Chem. Rev.*, 2015, **115**(24), 13165–13307.

47 S. Eskandari, T. Guerin, I. Toth and R. J. Stephenson, Recent advances in self-assembled peptides: Implications for targeted drug delivery and vaccine engineering, *Adv. Drug Delivery Rev.*, 2017, **110–111**, 169–187.

48 R. R. Khanikar, M. Kalita, P. Kalita, B. Kashyap, S. Das, M. R. Khan, *et al.*, Cold atmospheric pressure plasma for attenuation of SARS-CoV-2 spike protein binding to ACE2 protein and the RNA deactivation, *RSC Adv.*, 2022, **12**(15), 9466–9472.

49 J. M. Antosiewicz and D. Shugar, UV–vis spectroscopy of tyrosine side-groups in studies of protein structure. Part 2: selected applications, *Biophys. Rev.*, 2016, **8**, 163–177.

50 P. Singh, R. K. Sharma, O. P. Katare and N. Wangoo, Understanding tyrosine self-assembly: from dimer assembly to magnetized fluorescent nanotubes embedded into PVA films, *Mater. Adv.*, 2022, **3**(16), 6518–6528.

51 J. M. Antosiewicz and D. Shugar, UV–vis spectroscopy of tyrosine side-groups in studies of protein structure. Part 1: basic principles and properties of tyrosine chromophore, *Biophys. Rev.*, 2016, **8**, 151–161.

52 J. Feitelson, On the Mechanism of Fluorescence Quenching. Tyrosine and Similar Compounds, *J. Phys. Chem.*, 1964, **68**(2), 391–397.

53 P. Larkin, *Infrared and Raman Spectroscopy: Principles and Spectral Interpretation*, 1st edn, 2011.

54 M. Annadhasan, T. Muthukumarasamyvel, V. R. Sankar Babu and N. Rajendiran, Green Synthesized Silver and Gold Nanoparticles for Colorimetric Detection of Hg^{2+}, Pb^{2+}, and Mn^{2+} in Aqueous Medium, *ACS Sustain. Chem. Eng.*, 2014, **2**(4), 887–896.

55 E. Takai, T. Kitamura, J. Kuwabara, S. Ikawa, S. Yoshizawa, K. Shiraki, *et al.*, Chemical modification of amino acids by atmospheric-pressure cold plasma in aqueous solution, *J. Phys. D Appl. Phys.*, 2014, **47**(28), 285403.

56 J. K. Lin, K. J. Chen, G. Y. Liu, Y. R. Chu and S. Y. Lin-Shiau, Nitration and hydoxylation of aromatic amino acid and guanine by the air pollutant peroxyacetyl nitrate, *Chem. Biol. Interact.*, 2000, **127**(3), 219–236.

57 E. R. Stadtman and R. L. Levine, Free radical-mediated oxidation of free amino acids and amino acid residues in proteins, *Amino Acids*, 2003, **25**(3–4), 207–218.

58 E. A. Permyakov, The Use of UV–vis Absorption Spectroscopy for Studies of Natively Disordered Proteins, *Intrinsically Disordered Protein Analysis: Methods in Molecular Biology*, Humana Press, Totowa, NJ, 2012, vol. 895, pp. 421–433.

59 S. Mourdikoudis, R. M. Pallares and N. T. K. Thanh, Characterization techniques for nanoparticles: comparison and complementarity upon studying nanoparticle properties, *Nanoscale*, 2018, **10**(27), 12871–12934.

60 A. Oake, P. Bhatt and Y. V. Pathak, Understanding Surface Characteristics of Nanoparticles, in *Surface Modification of Nanoparticles for Targeted Drug Delivery*, Springer International Publishing, Cham, 2019, pp. 1–17.

61 C. Schneider, L. Gebhardt, S. Arndt, S. Karrer, J. L. Zimmermann, M. J. M. Fischer, *et al.*, Acidification is an essential process of cold atmospheric plasma and promotes the anti-cancer effect on malignant melanoma cells, *Cancers*, 2019, **11**(5), 671.

62 X. Zhang, R. Zhou, K. Bazaka, Y. Liu, R. Zhou, G. Chen, *et al.*, Quantification of plasma produced OH radical density for water sterilization, *Plasma Processes Polym.*, 2018, **15**(6), 1700241.

63 T. W. Chen, C. T. Liu, C. Y. Chen, M. C. Wu, P. C. Chien, Y. C. Cheng, *et al.*, Analysis of Hydroxyl Radical and Hydrogen Peroxide Generated in Helium-Based Atmospheric-Pressure Plasma Jet and in Different Solutions Treated by Plasma for Bioapplications, *ECS J. Solid State Sci. Technol.*, 2020, **9**(11), 115002.

64 K. Oehmigen, J. Winter, M. Hähnel, C. Wilke, R. Brandenburg, K. D. Weltmann, *et al.*, Estimation of Possible Mechanisms of Escherichia coli Inactivation by Plasma Treated Sodium Chloride Solution, *Plasma Processes Polym.*, 2011, **8**(10), 904–913.

65 H. Tresp, M. U. Hammer, K. D. Weltmann and S. Reuter, Effects of Atmosphere Composition and Liquid Type on Plasma-Generated Reactive Species in Biologically Relevant Solutions, *Plasma Med.*, 2013, **3**(1–2), 45–55.

66 J. M. Souza, Q. Chen, B. Blanchard-Fillion, S. A. Lorch, C. Hertkorn, R. Lightfoot, *et al.*, Reactive Nitrogen Species and Proteins: Biological Significance and Clinical Relevance, in *Biological Reactive Intermediates VI*, Springer, Boston, MA, 2001, vol. 500, pp. 169–174.

67 J. L. Zweier, A. Samouilov and P. Kuppusamy, Non-enzymatic nitric oxide synthesis in biological systems, *Biochim. Biophys. Acta Bioenerg.*, 1999, **1411**(2–3), 250–262.